Journal of Biomedical Materials Research Part A

WILEY

Society For Biomaterials

RESEARCH ARTICLE OPEN ACCESS

Coaxial Electrospinning of Multicomponent Fiber Membranes for Sustained Oxygen Supply in Hypoxic Environment

Brooke Campbell[1] | Houra Mobaleghaleslam[1] | Robert Horvath[1] | Daewoo Han[1] | Hiroyuki Kato[2] | Hirotake Komatsu[2] | Andrew J. Steckl[1]

[1]Nanoelectronics Laboratory, Department of Electrical and Computer Engineering, University of Cincinnati, Cincinnati, Ohio, USA | [2]Department of Surgery, University of California San Francisco, San Francisco, California, USA

Correspondence: Andrew J. Steckl (a.steckl@uc.edu)

Received: 22 April 2026 | **Revised:** 11 August 2026 | **Accepted:** 14 August 2026

Keywords: calcium peroxide | coaxial electrospinning | fiber membranes | hypoxia | oxygen-generating material | pancreatic beta cells

ABSTRACT

A major challenge for cell and tissue transplantation is providing a sustaining environment for newly transplanted cells and tissues. They require a temporary oxygen source since newly transplanted cells and tissues are not yet connected to the recipient's vascular system. Here we report on core-sheath fiber membranes formed using the coaxial electrospinning process that contain calcium peroxide (CPO) embedded in the fiber core to provide a source of oxygen by diffusion from the fibers over a period of multiple days. Embedding the enzyme catalase in the fiber sheath as a catalyst is found to significantly reduce the production of cytotoxic hydrogen peroxide (H_2O_2) by ~59% and to increase the overall amount of oxygen released up to ~28% after 4 days of release. CPO-containing PCL/PVP-PEO core-sheath fiber membranes produced enhanced cell viability of > 90% at Day 5 for metabolically active pancreatic beta cell spheroids in a hypoxic environment, while non-CPO control cases resulted in no surviving cells at Day 5. Preliminary investigations with the incorporation of lysozyme as a model protein in the fiber core for eventual growth factor incorporation have yielded promising sustained release of lysozyme up to 10 days.

1 | Introduction

Oxygen availability is a critical parameter for cellular metabolism and viability [1, 2]. In particular, during cell transplantation, insufficient oxygen supply without vascularization significantly limits successful outcomes [3, 4]. Consequently, strategies that enable localized, sustained, and controllable oxygen delivery have emerged to maintain cellular functions after transplantation until they are properly vascularized in a recipient tissue [5, 6].

Electrospinning is a fiber microfabrication process that is economical, versatile, and adaptable to high throughput manufacturing [7]. Electrospun fibrous membranes have characteristics similar to those of the extracellular matrix in tissues, with the micro- and nano-scale structures of the fibers having a profound effect on cell growth, enhancing cell adhesion, proliferation, migration, and differentiation [8, 9]. Electrospun membranes can provide enhanced cytocompatibility by supporting cell attachment and proliferation by easily adjusting their composition, fiber structure, surface properties, and incorporated functional molecules [10, 11].

Homogenous fibers can be formed from a single spinneret nozzle, or core-sheath fibers can be formed using a coaxial nozzle, with the outer polymer enveloping the inner polymer,

Brooke Campbell and Houra Mobaleghaleslam contributed equally to this study.

as seen in Figure S1. Coaxial electrospinning of complex fiber membranes has been successfully applied to many bio/medical conditions, including coaxial fibers for local delivery of antitumor immunosuppressant (MPA) for brain tumors and coaxial fibers made up of a PVP/BSA/rhTGF-β1 core and PCL sheath to support bone marrow-derived stem cell adhesion and proliferation [12, 13]. Current electrospinning strategies to effectively deliver oxygen include electrospinning oxygen-generating nanofiber scaffolds which incorporate calcium peroxide (CPO–CaO_2) as an oxygen source to promote healthy tissue integration or supporting the health of aquatic organisms in hypoxic environmental waters [14–19]. Other strategies include nanofibers loaded with sodium percarbonate as an oxygen source to address wound healing, or support stem-cells in cell-based skin-tissue engineering and bone regeneration [20–22]. Zhang et al. used electrospun core-sheath chitosan fibers loaded with perfluorotributylamine (PFTBA) to deliver oxygen in a hypoxic environment for the repair of intervertebral discs in rats [23]. Ma et al. utilized core-sheath polycaprolactone (PCL) fibers to deliver oxygen for nerve regeneration [24]. In this study, we report on a delivery system using coaxially electrospun multifunctional bioagents to address oxygen and vascular needs in cell and tissue transplantation. To date multifunctional coaxial fibers have yet to be developed as a potential therapy for cell transplantation to induce angiogenesis while simultaneously meeting the initial oxygen demand of the newly grafted cells.

Materials utilized in biomedical applications to deliver oxygen in a hypoxic environment [25] include calcium peroxide (CPO—CaO_2), sodium percarbonate (SPC—2 $Na_2CO_3 \cdots 3\ H_2O_2$), and perfluorotributylamine (PFTBA—$N(CF_2CF_2CF_2CF_3)_3$). CPO has a higher water solubility and releases more oxygen compared to SPC. CPO has two pathways to produce oxygen, with release kinetics dependent on pH and temperature [26]. CPO can react with water to form oxygen directly without the intermediate formation of hydrogen peroxide following pseudo-first-order kinetics (Equation 1), with the reaction rate decreasing as CaO_2 is consumed. The second reaction follows pseudo-zero-order kinetics, where the reaction rate is an artifact of the conditions under which the reaction is carried out. Reactions (1) and (2) form a parallel reaction system and compete with each other. Increasing pH at a given temperature increases the O_2 yield while decreasing the H_2O_2 yield [26].

$$\text{Pseudo} - \text{first} - \text{order kinetics: } CaO_2 + H_2O \rightarrow Ca(OH)_2 + 1/2O_2 \quad (1)$$

$$\text{Pseudo} - \text{zero} - \text{order kinetics: } CaO_2 + 2H_2O \rightarrow Ca(OH)_2 + H_2O_2 \quad (2)$$

Since hydrogen peroxide can cause cell cytotoxicity, it is imperative to increase the rate of conversion of generated hydrogen peroxide into oxygen [27] The catalase enzyme is a naturally occurring enzyme found in the body, which is responsible for decomposing reactive-oxygen species (ROS) into water and oxygen via the following reaction: $2H_2O_2 \rightarrow 2H_2O + O_2$. Therefore, the catalase not only protects cells from the damage caused by ROS but also provides more oxygen from hydrated CaO_2. The other by-product of the reaction, calcium hydroxide [$Ca(OH)_2$], is a strong base (pH ~12–13) that can negatively affect cells. To reduce possible cytotoxic effects of calcium hydroxide, one can incorporate buffering salts or polymers, such as alginate and sodium citrate, into the electrospinning solution that would provide eventual buffering capability against calcium hydroxide.

The oxygen generation mechanism in our core-sheath electrospun membrane is based on the hydrolysis of CaO_2 incorporated within the core layer. The process starts with gradual dissolution of the PEO sheath in core-sheath fibers. Upon exposure to the aqueous environment, CaO_2 particles in the core react with water to generate oxygen (O_2), hydrogen peroxide (H_2O_2), and calcium hydroxide ($Ca(OH)_2$). The generated oxygen then diffuses through the polymer matrix and the interconnected pores formed as the hydrophilic PVP/PEO components hydrate and dissolve. The controlled water penetration and controlled oxygen diffusion combine to minimize burst release and enable sustained oxygen release over an extended period.

A critical restricting factor in cell and tissue transplantation is lack of oxygenation, which occurs due to the absence of blood vessels to the newly transplanted cells [28, 29]. Angiogenesis, the process in which new blood vessels are formed, is required to establish a stable oxygen supply and typically occurs in 7–10 days [30, 31] Here, we report that the combined release of CPO/catalase/lysozyme provides a sustainable oxygen supply for more than 15 days, and the potential for the long-term release of growth factors using a model protein.

2 | Experimental

2.1 | Fabrication of Oxygen-Releasing Fibers

The polymers poly(ε-caprolactone) (PCL), polyvinylpyrrolidone (PVP), and polyethylene oxide (PEO) were selected due to their combined excellent biocompatibility, suitable electrospinnability, and complementary degradation characteristics. PEO was incorporated to enhance the degradation rate of the sheath layer. The core contained mainly PCL to provide structural stability and regulate the oxygen release from CaO_2. PVP was also introduced into the core to accelerate the oxygen release.

PCL ($CH_3(C_6H_{10}O_2)_nCH_3$, $M_n = 80$ kDa), PVP ($((C_6H_9NO)_n$, $M_w = 1.3$ MDa), and PEO ($(-CH_2CH_2O-)_n$, Mw = 100 kDa) were purchased from Sigma-Aldrich (St. Louis, MO). Calcium peroxide (75%, 200 mesh), catalase (from bovine liver, 2000–5000 U/mg), and fluorescein 5(6) isothiocyanate were also purchased from Sigma-Aldrich. Solvents such as 2,2,2-trifluoroethanol (TFE, 99.8%, CF_3CH_2OH, extra pure) were purchased from Fisher Scientific (Waltham, MA).

For preparation of the core solution, CPO was first dispersed in TFE at a concentration of 25 mg/mL and sonicated for 15 min to obtain a homogeneous suspension. Subsequently, 9% (w/v) PCL and 3% (w/v) PVP were added to the suspension. For preparation

TABLE 1 | List of samples and coaxial electrospinning parameters.

Core				Sheath					
Polymers and conc. (%)	CPO (mg/mL)	Protein (mg/mL)	Solvent	Polymers and conc. (%)	Catalase (mg/mL)	Solvent	Voltage (kV)	Core/sheath flow rate (mL/h)	Sample name
PCL/PVP (75:25) [12%]	—	—	TFE	PEO [10%]	—	TFE	15	1.0/0.2	Control
PCL/PVP (75:25) [12%]	25[a]	—	TFE	PEO [10%]	—	TFE	15	1.0/0.2	CPO
PCL/PVP (75:25) [12%]	25	—	TFE	PEO [10%]	0.5	TFE	15	1.0/0.2	CPO + Catalase
PCL/PVP (75:25) [12%]	25	0.3	TFE	PEO [10%]	0.5	TFE	15	1.0/0.2	CPO + Catalase + Protein

Note: Concentrations given are for starting solutions.
[a]Equivalent to 2.5 w/v%.

of the sheath solution, catalase was dissolved in TFE at a concentration of 0.5 mg/mL and sonicated for 15 min. After complete dispersion, 10% (w/v) PEO was added to the solution. Finally, both the core and sheath solutions were placed on a rotator and mixed overnight at room temperature to ensure complete polymer dissolution and homogeneous distribution of all components before electrospinning.

The electrospinning operation utilized a NE-1000 syringe pump (New Era Pump System) to control the flow of polymer solutions. A coaxial 22-gauge inner needle (0.711 mm OD, 0.406 mm ID) with an 18-gauge outer needle (1.24 mm OD, 0.84 mm ID) was used for core-sheath fiber formation. The nozzle apex-to-collector distance of 22 cm was generally used in a standard electrospinning configuration, as shown in Figure S1. Taylor cone formation and liquid jet extraction were achieved by applying a DC voltage (Glassman Series EL) of typically 15 kV. Table 1 lists the sample materials (host polymer, solvent, and embedded component) and respective concentrations. The core solution was prepared by dissolving PCL/PVP and lysozyme and dispersing CPO in TFE. The sheath solution was also prepared by dissolving PEO and catalase in TFE. The solution flow rates were 1.0 and 0.2 mL/h for core and sheath solutions, respectively. The prepared membrane showed a uniform appearance and was mechanically robust to handle. The thickness of electrospun membranes was typically ~100 μm and membrane area ranged from 25 cm^2 for small membranes to 500 cm^2 for larger sizes.

2.2 | Characterization

2.2.1 | Fiber Morphology

Samples were Au-sputtered for 60s using a Desk V sputter system (Denton Vacuum) prior to imaging using electron microscopy. SEM images were acquired using the FEI Aereo LoVac SEM (ThermoFisher) at various magnifications using a voltage of 10 kV and a current of 0.10 nA. The TEM sample was prepared by electrospinning the membrane directly onto the copper TEM grid. TEM images were acquired using the Talos F200i (ThermoFisher) with an acceleration voltage of 200 kV.

2.2.2 | Measurement of Oxygen Release Kinetics

For measurement of oxygen and protein release kinetics, samples with $7 \times 7\ mm^2$ area and 100 μm thickness were sectioned out of the fabricated membrane using a straight-edge razor. Oxygen concentration was measured using a fiber-optic microsensor (Pyroscience OXROBSC model). Samples were placed inside a 2 mL glass vial with a sealed cap. The sample vials were filled with 1.5 mL of Dulbecco's phosphate buffered saline (DPBS) solution with pH of 7.23 at ~21°C. Oxygen concentration was measured at 21°C every 24 h by opening the container cap, inserting the probe inside the solution, taking the measurement, and then closing the container. This measurement process takes approximately 10 min. Five independent experiments were performed in parallel for each case ($n = 5$), and the data reports the average value and standard deviation (SD). Although brief exposure to air during daily measurements may have allowed limited oxygen exchange with the atmosphere, all groups were measured under identical conditions. Therefore, the current setup provided a consistent platform for comparing oxygen release, although it does not fully replicate the in vivo environment. For the future, we plan to use a closed vial measurement configuration using remote sensing of the oxygen concentration.

2.2.3 | Measurement of Hydrogen Peroxide Release Kinetics of Oxygen-Releasing Fibers

Hydrogen peroxide concentrations were determined using Amplex Red Hydrogen Peroxide Assay Kit (Invitrogen) and BioTek Synergy H1 plate reader (Agilent Technologies) with excitation at 517 nm and emission at 585 nm. Ten microliter of sample solution was taken from the sample vials and used according to the manufacturer's instructions for hydrogen peroxide concentration assessment in sample solutions.

2.2.4 | Measurement of Protein Release Kinetics of Oxygen-Releasing Fibers

Lysozyme is a small, single-chain protein (~14 kDa). It was selected as a model protein, for the eventual incorporation of

growth factor proteins (such as VEGF with a similar size of 18–20 kDa/monomer) for enhancing vascularization. Lysozyme was labeled with FITC (Sigma Aldrich) according to standard procedure (Supporting Information). After a day of incubation (described in the Section 2.2.2), 0.5 μL of solution from sample vials were transferred to the 96-well plate. The amount of protein released from the fiber membrane was measured using a plate reader (BioTek Synergy H1 plate reader; Agilent Technologies) with excitation peak at 495 nm and emission peak at 519 nm.

To evaluate the effect of CPO release and hydrolyzation in pH that may affect protein and/or cells present, pH measurements of DI water and DPBS solutions containing various membranes (CPO, CPO + catalase, control) were performed over multiple days as shown in Figure S2. The pH remained stable in the 7.04–7.07 range, indicating that the incorporation and release of CPO and catalase in membranes did not appreciably alter the pH of the surrounding medium.

2.3 | Cell Culture Studies With Oxygen-Releasing Fibers

2.3.1 | Production of Three-Dimensional (3D) Spheroids

A rat beta cell line (INS-1 832/3 Rat Insulinoma Cells, Sigma Aldrich) was used to produce 3D spheroidal cell structures. Cells were expanded in a 2D tissue culture-treated flask with RPMI1640 media (500 mL, ATCC, San Diego, CA) supplemented with 10% heat-inactivated fetal bovine serum (FBS, Gibco), 20 μL of 1 M 2-mercatoethanol (Sigma Aldrich), and 1% antibiotics (Gibco). Trypsinized single cells were seeded onto a 35 mm microwell plate (EZSPHERE 900SP; 500 μm microwell diameter; Nacalai USA, San Diego, CA) at a seeding density of 1.25×10^6 cells/well. The microwell plate was incubated at 5% CO_2 and 37°C for 72 h to form the spheroids in ~100–150 μm diameter. Spheroids were then collected for subsequent hypoxic experiments described in Section 2.3.3.

2.3.2 | Morphology of Spheroids

AnaSP and ReViSP opensource software programs (originally scripted in MATLAB) were used to determine spheroid morphological metrics including circularity, solidity, and sphericity. Through segmentation, AnaSP creates a binary mask based on the brightfield image of a spheroid; from the resulting mask, AnaSP calculates several spheroid parameters while ReViSP creates a 3D rendering of the spheroid.

2.3.3 | Preparation of Hypoxic Environment

A modular hypoxic incubator chamber (Embrient Inc., San Diego, CA) was used to induce a hypoxic environment surrounding the spheroids. The chamber was purged using a certified-pure hypoxic gas mixture (Wright Brothers, Cincinnati, OH) composed of 1% oxygen, 5% carbon dioxide, and 94% nitrogen. Oxygen levels inside the incubator were verified using the F-950 3-gas analyzer (Felix Instruments, Camas, WA) via a 3D-printed rubber septum stopper. To maintain humidity within the hypoxic chamber, a Petri dish containing sterile gauze saturated with sterile water was placed in the lower section of the hypoxic chamber.

2.3.4 | Effectiveness of Membrane Assessment in Hypoxic Condition

For cell-based measurements 6 × 6 mm membrane pieces were sectioned and placed in the bottom of a Costa ultra-low attachment 96-well plate to determine the feasibility and effectiveness of the oxygen-releasing membrane. A 20-min UV-C cycle (Philips Hue UV Light Sanitizer Box) was utilized to sterilize the fiber membranes prior to spheroid seeding. Spheroids were seeded on top of membranes in each well with a seeding density of 50 spheroids/well and 200 μL of RPMI media, as follows: illustrated in Figure S3. The well plate was placed into the hypoxic chamber, and the chamber lid was fastened using a spring-loaded O-ring clamp. The chamber was then purged with hypoxic gas for 3 h using a flow meter set at 1.5 SCFH (708 sccm). Prior to sealing the gas inlet and outlet tubes, the oxygen and carbon dioxide content inside the chamber was verified using the three-gas analyzer. Once verified, the modular hypoxic chamber was placed inside the incubator at 37°C under 5% CO_2 environment. Figure 1 illustrates the hypoxic experimental process.

2.3.5 | Viability Assessment of Spheroids Using Image Analysis

Live/dead staining of the spheroids was used to assess cell viability after 1, 3, and 5 days of incubation in a hypoxic chamber. First, spheroids were collected via pipette from the well-plate. Second, the spheroids were incubated for 5 min in a dark environment in 400 μL Dulbecco's phosphate-buffered saline (DPBS) containing 4 μL of fluorescein diacetate (FDA, 5 mg/mL) and 4 μL of propidium iodide (PI, 1 mg/mL). All materials were purchased from Sigma Aldrich (St. Louis, MO). After incubation, spheroids were washed with DPBS and then transferred to an ultra-low attachment 24-well plate to capture the fluorescent images using a Leica DMi8 widefield fluorescent microscope. A total of 20 spheroids from each group were analyzed. Spheroids smaller than 100 μm and larger than 200 μm were excluded from analysis. ImageJ was used to define the total area of the spheroid, the PI-stained necrotic areas (red), and the FDA-stained live areas (green). Viability of individual spheroids was calculated using a two-dimensional area-based analysis according to the following equation:

$$\text{Viability}\,(\%) = 100 \times \text{FDA} - \text{positive area} / (\text{FDA} - \text{positive area} + \text{PI} - \text{positive area}).$$

Overall viability for each experimental group was calculated as the mean viability of the 20 analyzed spheroids.

2.4 | Statistical Analysis

All statistical data were presented as mean ± standard deviation (SD). Number of samples were noted in each data set

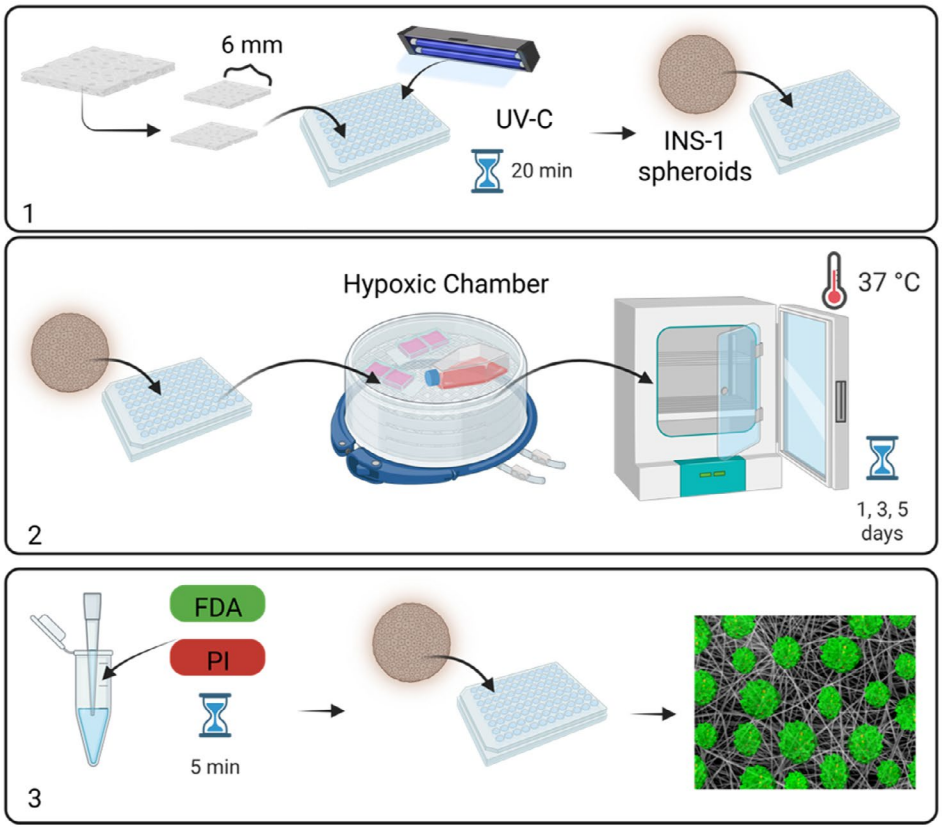

FIGURE 1 | Spheroid hypoxic experimental procedure. FDA, fluorescein diacetate, live cell indicator; PI, propidium iodide, dead cell indicator dye. Membrane size—$6 \times 6\,mm^2$. (1) Sample preparation, (2) hypoxic incubation, and (3) viability assay.

and figure. Especially for Figure 8, spheroid necrosis (%) was quantified from confocal fluorescence images and analyzed using two-way ANOVA ($n = 20$) with treatment and time as independent parameters, followed by Tukey's multiple comparisons test.

3 | Results and Discussion

3.1 | Fiber Morphology

PCL/PVP core and PEO sheath fiber membranes were produced with CPO/catalase in core and lysozyme in sheath, as shown in Figure 2. For comparison, control membranes were produced containing only polymers. The fiber morphology, diameter, and structure of the electrospun core-sheath fiber membranes were observed using SEM and TEM. SEM images in Figure 2 show the presence of randomly oriented fibers with varying diameters (average diameter of ~1.08 μm and SD of ~0.38 μm), with no beads being formed during the electrospinning process (Figure 2a). Some CPO particles embedded in the fibers can be seen on the fiber surface, indicated by the yellow box (Figure 2b). A secondary jet was occasionally emitted from the Taylor cone during electrospinning, yielding fibers with a substantially smaller diameter (Figure 2b–d). TEM images confirm the presence of core-sheath fibers in Figure 2e,f presenting a ~50 nm fiber core surrounded by a 60–70 nm thick sheath leading to a total fiber diameter of ~175 nm.

3.2 | Release Kinetics: Oxygen and Hydrogen Peroxide

As indicated in Section 2.2.2 the oxygen concentration was measured daily for the three membrane types (control, CPO, CPO/catalase) as well as for the plain DPBS solution (no membrane). The net daily O_2 concentration in solution (1.5 mL) for all four cases is shown in Figure 3a over a period of 2 weeks. At the start of the measurements, the O_2 concentration for DPBS solution is ~7.5 μg/mL, which is in the ~7–8 μg/mL range to be found in DPBS solutions near room temperature [32]. The control membrane, which contains no CPO, yields a similar background O_2 concentration of ~8.4 μg/mL on Day 0. In Figure 3, the measured O_2 concentration in DPBS solution ("background") was subtracted for all measured O_2 concentrations from membrane samples to evaluate the oxygen released from the membranes.

The daily O_2 release amounts (μg) by the $7 \times 7\,mm^2$ membrane samples and corresponding O_2 release amount/per membrane unit area (μg/cm^2) are shown in Figure 3b. The size of membrane samples was dictated by the available space for implantation in mice. The actual amount of oxygen released needs to be consistent with the number of islets to be implanted. At Day 0, the CPO and CPO/catalase membranes produce a significantly higher O_2 concentration of ~21.2 and ~26.1 μg, respectively, compared to ~1.7 μg for control membranes. The corresponding O_2 release per membrane unit area for the CPO and CPO/catalase cases are 43.3 and 53.3 μg/cm^2, respectively. After this initial "fast release", the

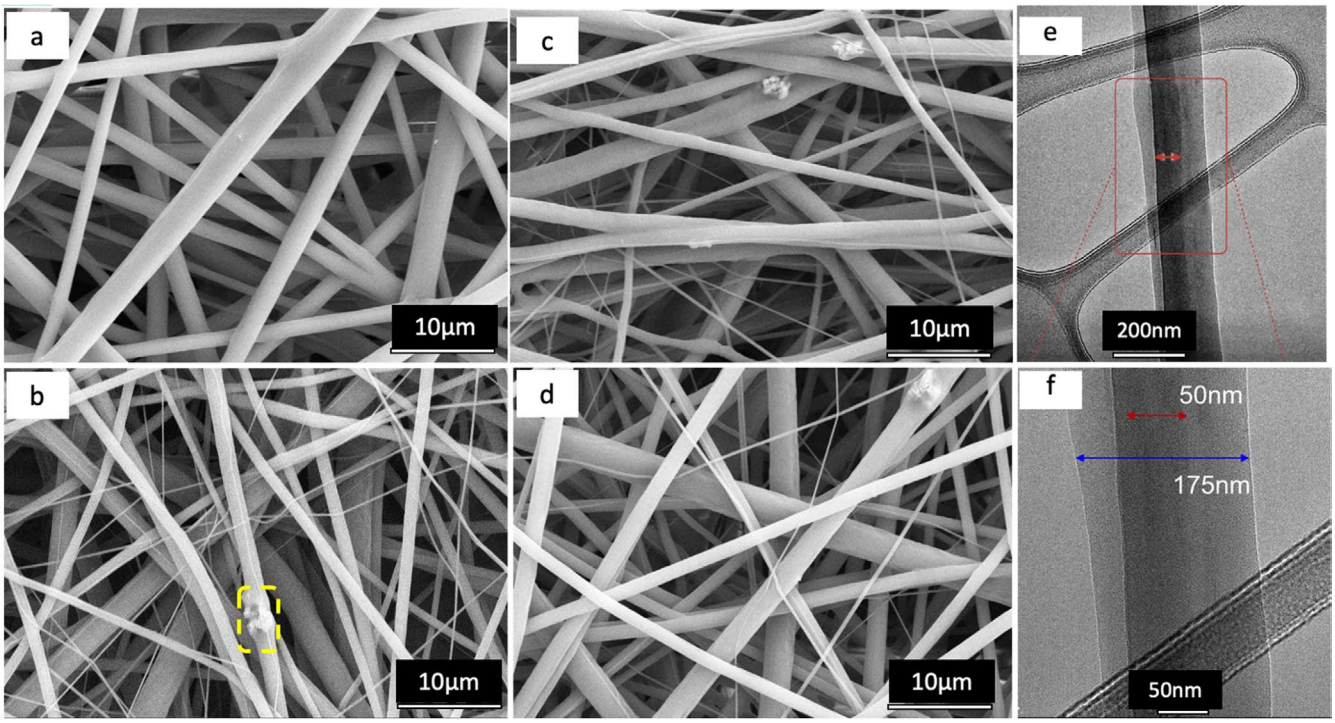

FIGURE 2 | Morphology and dimensions of coaxially electrospun core-sheath fibers—SEM images of (a) control membrane at ×3k; (b) membrane with embedded CPO particle visible; (c) CPO/catalase membrane; (d) CPO/catalase/protein membrane. TEM images of thin fiber of control membrane at (e) ×58k; (f) ×245k.

CPO-containing membranes exhibit a reduced but consistent O_2 release, which is higher than that of the control membranes. After the fast release on Day 0, there is a "bump" release covering the first 5 days after which the net additional release is fairly low and relatively constant. This initial bump release is very important since this initial period is the most critical time demanding high oxygen supply to newly transplanted cells.

A clearer comparison between the membrane types is obtained by examining the cumulative O_2 amount released into solution over the 2-week period. As shown in Figure 3c, the total amount of O_2 released increases with time for all cases. The CPO/catalase membranes display a uniformly higher O_2 release over time than the CPO-only membrane, indicating the functionality of the catalase-driven conversion of H_2O_2 to O_2.

To highlight the effect of the CPO embedded into the fiber membranes, we evaluate the amount of oxygen released considering the number of islets that can be properly provided with oxygen during the first couple of weeks after being transplanted. On Day 0 the CPO-only and the CPO/catalase membranes with $7 \times 7\,mm^2$ area and 0.1 mm thickness released a net O_2 amount of ~21.2 and 26.1 μg, respectively. Over the first 5 days the corresponding cumulative O_2 released is ~54 and 75 μg, respectively. The daily oxygen release rates from CPO-only and CPO/Catalase membranes averaged over 14 days are ~8.9 and ~11.1 μg/day. For comparison, the cumulative amount of oxygen required by 50 and 100 islets based on consumption of 1 pmol/min per islet [33] is equivalent to ~2.5 and 5 μg per day, respectively. Clearly, both CPO-containing membranes provide a sufficient amount of oxygen, with the CPO + catalase membrane being able to support ~220 islets (25%–30% more than the CPO-only membrane).

Next, the effect of incorporation of catalase in the CPO-containing membranes on the production of hydrogen peroxide and oxygen is considered. The cumulative H_2O_2 amount released in solution over a period of 14 days is shown in Figure 4a and the corresponding O_2 release is shown in Figure 4b. Embedding catalase into the CPO membranes results in marked reduction (~58.5%) in the released amount of H_2O_2 and an accompanying increase (~28%) in O_2 release. This confirms that the catalase incorporated into the electrospun fiber membranes performs the catalytic reaction of converting H_2O_2 to O_2, increasing oxygen production. This also provides the useful side effect of protecting cells from the damage caused by ROS. Interestingly, even though catalase dissolved in TFE was reported [34] to be denatured during the electrospraying process in this case using electrospinning the catalase appears to have maintained its enzymatic effect (Figure 4).

The increased oxygen and reduced hydrogen peroxide levels are consistent with catalase-mediated decomposition of hydrogen peroxide. While our results shown in Figure 4 support a catalase-mediated mechanism, other possible variables such as pH and temperature may contribute to the increased oxygen level [26]. Future studies using direct catalase activity measurements will be conducted to confirm this mechanism conclusively.

3.3 | Release Kinetics: Protein Membrane

As indicated previously (Section 2.2.4), lysozyme was selected as a model protein for the eventual incorporation of growth factor proteins for enhancing vascularization. Lysozyme labeled with FITC fluorescent dye for evaluating the release kinetics was incorporated into the core of the fibers along with CPO and catalase. The

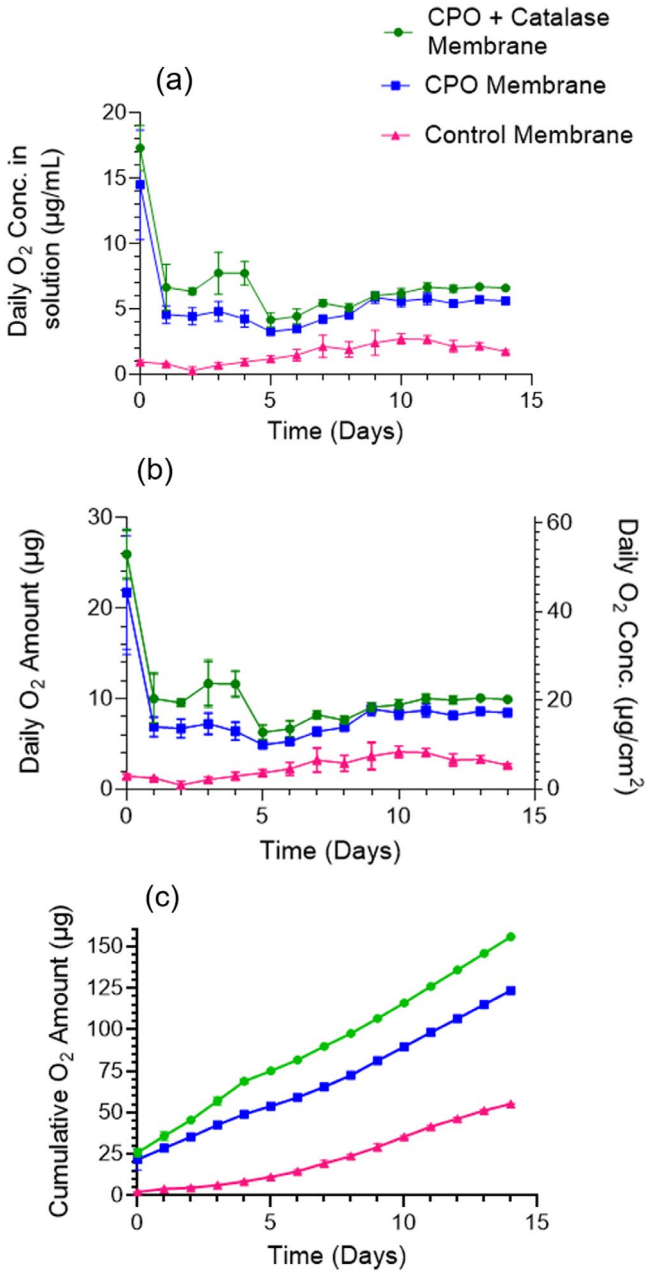

FIGURE 3 | Oxygen release from several types of 2.5% CPO fiber membranes with 7×7 mm^2 area (with subtraction of no-membrane case): (a) daily O_2 concentration in solution (μg/mL); (b) daily amount released (μg, μg/cm^2); (c) cumulative O_2 released (μg). $n = 5$ for all sample groups.

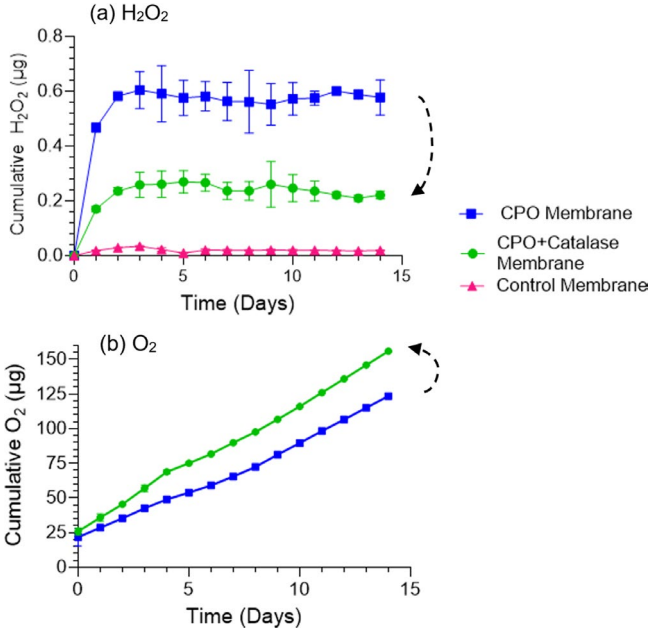

FIGURE 4 | Effect of catalase (shown as the dashed arrow curves) on release kinetics of hydrogen peroxide and oxygen from 2.5% CPO fiber membranes (7×7 mm^2): (a) cumulative amount of hydrogen peroxide release (μg); (b) cumulative amount of oxygen release (μg). $n = 5$ for each sample group.

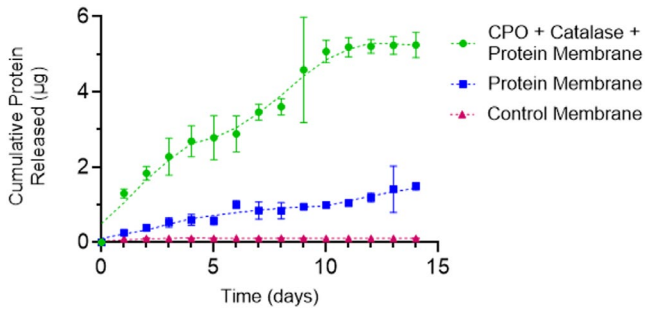

FIGURE 5 | Cumulative release of protein from fiber membranes (7×7 mm^2) placed in 1.5 mL of DPBS within sealed container. CPO + Catalase + Protein membranes contain 2.5% CPO, 0.5 mg/mL catalase, 0.3 mg/mL lysozyme (FITC). Protein membranes only contain lysozyme. Control membranes are unloaded. $n = 4$ for each sample group.

cumulative release of lysozyme into DPBS solution over a 2-week period is shown in Figure 5. The 7×7 mm^2 protein-only membrane released at a sustained rate of ~100 ng/day, reaching a total of ~1.5 μg over the 14-day period. Interestingly, the membranes that also contained CPO and catalase in addition to the protein released at a higher rate of ~0.5 μg/day for the first 10 days. After that point, these membranes released very little additional protein, saturating at ~5 μg total released amount. Assuming VEGF has similar release kinetics, replacing lysozyme with VEGF in future experiments, this concentration would be more than sufficient to reach the effective VEGF concentration (1–10 ng/mL) reported [35] for maximum endothelial cell growth activity.

Protein (lysozyme) release was statistically analyzed using Welch's *t*-test between two groups, which showed a significant difference ($p < 0.0001$) in protein release between the CPO + catalase group versus the protein-only group. The release kinetics of the protein from the fiber core are possibly affected by the chemical reaction of CPO also present in the fiber core. While oxygen is being produced and released, the host polymer fibers are mechanically weakened and chemically altered, allowing for a faster protein release than the protein-only membrane case. Additionally, increased ionic concentration in DPBS by released CPO and catalase may accelerate the release of proteins in fibers. Clearly, both membranes can provide consistent release of the model protein, lysozyme, over 14 days. Additional optimization of release rates and amounts will follow using animal models if necessary.

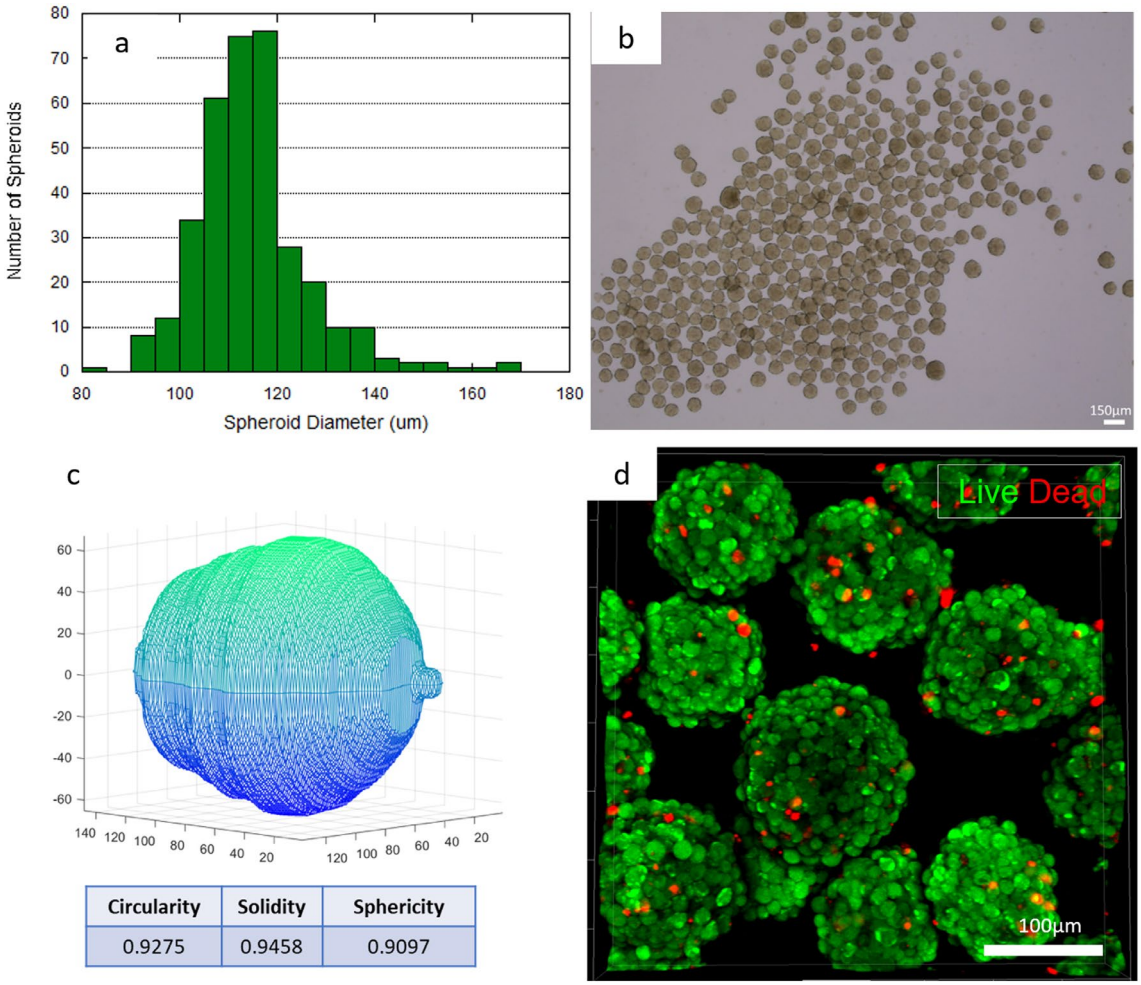

Circularity	Solidity	Sphericity
0.9275	0.9458	0.9097

FIGURE 6 | INS-1 cell spheroids: (a) spheroid size distribution; (b) optical brightfield image of clustered spheroids at ×4; (c) ANAsp-calculated spheroid parameters and ReViSP 3D render in microns; (d) confocal image of live (green, FDA)/dead (red, PI) stained spheroids at ×40.

Our findings demonstrate the ability of the nanofiber platform to encapsulate and release the model protein lysozyme and suggest its potential for growth-factor delivery for enhanced vascularization. Future work will directly evaluate VEGF encapsulation, release, and bioactivity followed by in vivo evaluation.

3.4 | Cellular Assessment

3D spheroids are emerging as a promising cell transplantation format because their pre-existing cell–cell contacts better preserve tissue-like architecture compared with single-cell transplantation, which eventually improves functional engraftment. Pancreatic islet transplantation exemplifies this strategy, utilizing intact spheroidal islets from cadaveric donors as well as stem cell-derived cell aggregates that form spheroid structures [36–39]. Native pancreatic islets reside in a highly oxygenated microenvironment in the pancreas [40]. Although islets account for only approximately 2% of the pancreatic volume, they receive nearly 10% of the total pancreatic blood supply [41].

Importantly, 3D spheroids inherently develop steep oxygen gradients toward their core due to diffusion limitations. Spheroids with an average diameter greater than 100 µm, comparable in size to pancreatic islets, are particularly vulnerable to hypoxia [28, 29]. In this study, we employed rat insulinoma (INS-1) cell spheroids as a model of oxygen-demanding 3D tissues relevant to transplantation.

3.4.1 | Spheroid Characterization

The formation of spheroids of INS-1 cells is described in Section 2.3.1. Collected spheroids show an average diameter of ~115 µm as seen in Figure 6a. Optical microscopy (Figure 6b) shows a collection of INS-1 spheroids consisting of uniform spheres. Figure 6c shows the AnaSP parameters generated from the spheroid mask and ReViSP 3D rendering. Cell aggregates analyzed using ImageJ software (National Institutes of Health, Bethesda, MD) yielded the following average parameters: circularity (CIR) of 0.93, sphericity index (SI) of 0.91, and solidity of 0.95. These values indicate [42] that the aggregates formed rounded shapes (CIR > 0.9), with high solidity (≥ 0.95) and spherical shape (SI ≥ 0.90). Confocal images with live/dead stained spheroids show uniform, dense spheres with minimal cell death and no necrotic core prior to the start of the hypoxic study (Figure 6d).

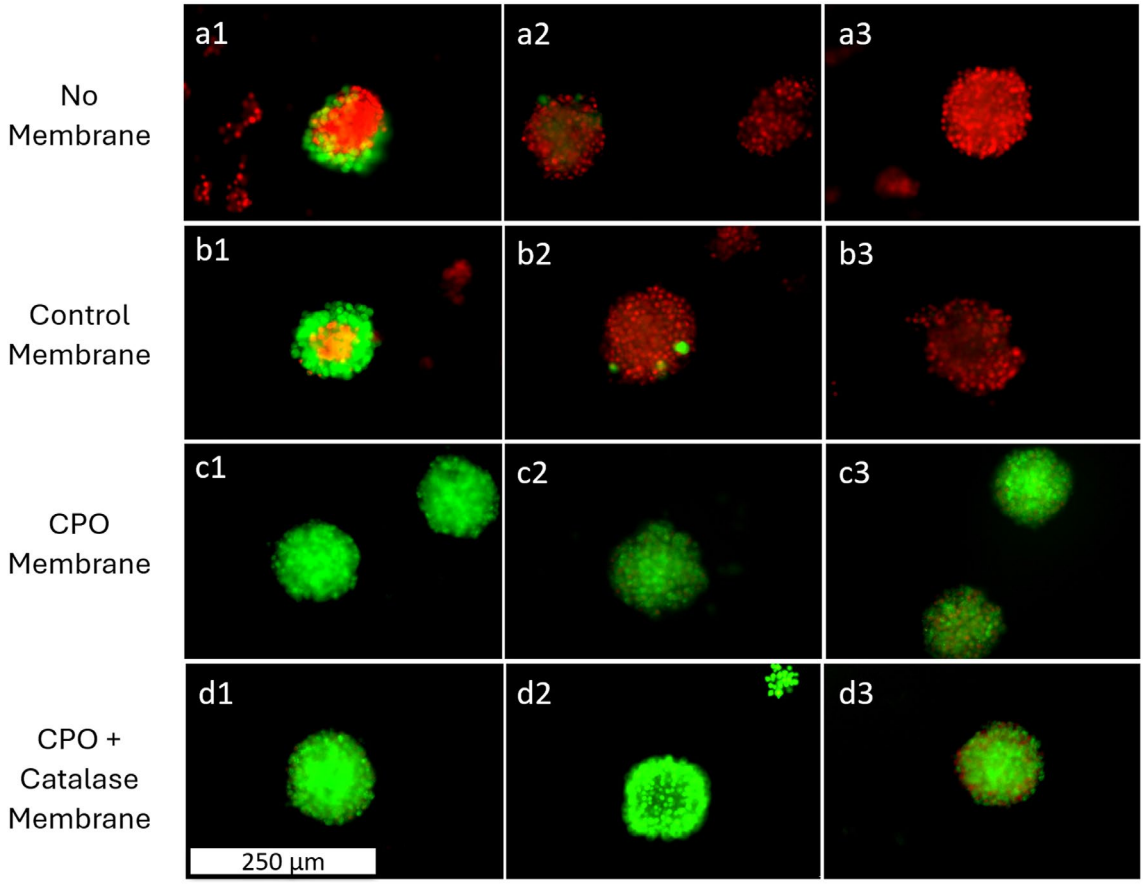

FIGURE 7 | Live/dead stained spheroids captured at ×10 magnification after 1-, 3-, and 5-day (columns 1, 2 and 3, respectively) incubation in a hypoxic environment: (a) spheroids freely seeded in media (without membrane); (b) spheroids seeded onto native (control) membrane; (c) spheroids seeded onto CPO membrane; (d) spheroids seeded onto CPO/catalase membrane.

3.4.2 | Cell Viability in Hypoxic Environment

The effect of CPO-embedded membranes has been evaluated for viability of spheroids in hypoxic conditions. Figure 7 illustrates the live/dead cell distribution in individual spheroids based on different membranes over several days. Figure 8 provides statistical analysis over 20 spheroids in each group. Spheroids seeded in media without a fiber membrane ("no membrane") showed significant cell death after 1 day of hypoxic incubation, with 38% of the spheroids (19 of 50) exhibiting necrotic features. Cell death originating from the center of the spheroid can be seen reaching the perimeter of the spheroid on the first day (Figure 7a1). Spheroids seeded onto the control membrane showed a 27.5% necrotic core of the spheroid (Figure 7b1). The CPO and CPO + catalase membrane show significantly reduced cell death after Day 1 hypoxia with only ~5.2% and ~1.2% cell death, respectively (Figure 7c1,d1). After 3 days of hypoxia exposure, the spheroids seeded without membranes showed ~93.3% cell death over the entire spheroid (Figure 7a2). Similarly, spheroids seeded onto the control membrane (no CPO) show 84% cell death with small patches of live cells throughout the cellular structure (Figure 7b2). However, spheroids seeded onto the CPO containing membranes exhibit a much reduced ~6.8% cell death, with the majority of the spheroid maintaining viable INS-1 cells (Figure 7c2). Spheroids seeded onto the CPO + catalase membrane show a similar result with ~8.9% cell death after 3 days of hypoxia exposure. After 5 days of hypoxia exposure both the spheroids in media-only and the spheroids seeded onto the native membrane showed complete cell death (Figure 7a3,b3). Many spheroids began to lose their circular shape and density due to the death of most INS-1 cells, as seen in Figure 7b3. In contrast, spheroids seeded onto the CPO and CPO + catalase membrane still show strong cell viability with only 10.3% and 11.4% cell death evenly distributed throughout the spheroid (Figure 7c3,d3).

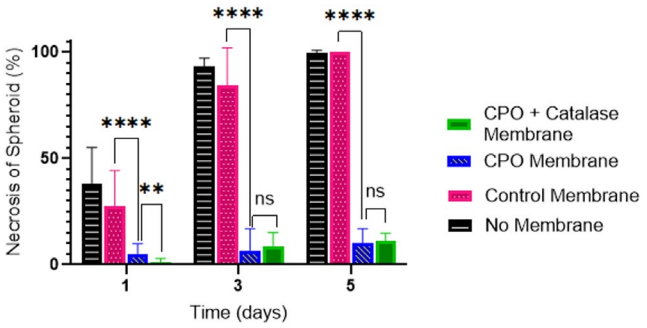

FIGURE 8 | Spheroid necrotic core percentage showing the effect of CPO membranes over several days. Statistical analysis using Welch's *t*-test between two groups ($n = 20$, spheroids are randomly selected for evaluation). ns $p > 0.05$, not significant; $^{**}p \leq 0.01$, very significant; $^{****}p \leq 0.0001$, extremely significant.

The necrotic core data for each case is shown in Figure 8 after Days 1, 3, and 5. A few qualitative observations are obtained: (a) necrotic core increases with the number of days for no membrane and control membrane cases, (b) the difference between No/Control membrane and CPO-containing membranes significantly increases with time. The statistical analysis was performed using Welch's *t*-test between two groups. The comparison between the Control and No membrane cases indicated statistical differences with p values ranging from 0.03 to 0.06. The comparison of Control membrane and CPO-containing membranes showed p-values < 0.0001, indicating extremely significant differences for all days. The presence of catalase in the membrane did play a role in the size of necrotic core only on Day 1 ($p < 0.01$). This is consistent with the effect of catalase on reducing H_2O_2 in the first 1–2 days (Figure 4a). From Day 3, the addition of catalase does not show a marked increase in spheroid viability in a hypoxic environment because the CPO membrane provides sufficient oxygen for present spheroids. However, we can expect that the CPO/catalase membrane will support a higher number of spheroids than that of the CPO membrane, considering the release kinetics discussed in Figure 3.

4 | Conclusions and Future Work

A multifunctional fiber membrane is demonstrated to be capable of simultaneous release of oxygen and proteins from coaxial fibers by incorporating CPO, catalase, and model protein into electrospun core sheath (PCL/PVP—PEO) fibers, which provide the oxygen for initial health of transplanted cells. Membranes with area of ~50 mm^2 and volume of ~5 mm^3 averaged over 14 days an oxygen release of 8.9 and ~11.1 μg/day from CPO-only and CPO/catalase membranes, respectively, with minimal amounts of cytotoxic reactive oxygen species (H_2O_2). These membranes effectively maintained spheroid viability in a hypoxic environment for 5 days without forming the necrotic core, demonstrating the potential to provide oxygen support to newly transplanted 3D cellular structures, such as pancreatic beta cells, until the vascularization around transplanted cells is established.

The configuration of our coaxial fibers produced a substantial initial release of oxygen followed by a tapered release, with spheroid data supporting that this release pattern effectively sustains INS-1 spheroids' viability. Suggested future work includes an inverted coaxial fiber design (a hydrophobic sheath, rather than a hydrophilic one) to evaluate if a more sustained release of oxygen further enhances INS-1 spheroid viability. Increasing CPO concentrations in fibers can provide sufficient oxygen levels in fiber membranes using a hydrophobic sheath. Additionally, further work is recommended to optimize simultaneous release of protein from coaxial fibers. While a model protein was used as proof of concept in this study, the next step is embedding VEGF into the fibers and evaluating effectiveness in promoting vascularization on transplanted spheroids/islets.

Author Contributions

The manuscript was written through contributions of all authors. All authors have given approval of the final version of the manuscript.

Acknowledgments

All authors appreciate funding support of this research by Breakthrough T1D (Grant 3-SRA-2023-1425-S-B). The authors at UCSF acknowledge the support of the Nora Eccles Treadwell Foundation. The authors at UC acknowledge the assistance of the Live Microscopy Core and Advanced Material Characterization Center.

Funding

This work was supported by the Breakthrough T1D (3-SRA-2023-1425-S-B) and Nora Eccles Treadwell Foundation.

Disclosure

No AI was used for preparation of this manuscript.

Conflicts of Interest

The authors declare no conflicts of interest.

Data Availability Statement

The data that support the findings of this study are available from the corresponding author upon reasonable request.

References

1. H. Komatsu, F. Kandeel, and Y. Mullen, "Impact of Oxygen on Pancreatic Islet Survival," *Pancreas* 47, no. 5 (2018): 533–543.

2. K. M. Shang, T. Suzuki, H. Kato, T. Toyoda, Y. C. Tai, and H. Komatsu, "Oxygen Dynamics and Delivery Strategies to Enhance Beta Cell Replacement Therapy," *American Journal of Physiology. Cell Physiology* 328, no. 5 (2025): C1667–c1684.

3. P. O. Carlsson, F. Palm, A. Andersson, and P. Liss, "Markedly Decreased Oxygen Tension in Transplanted Rat Pancreatic Islets Irrespective of the Implantation Site," *Diabetes* 50, no. 3 (2001): 489–495.

4. A. M. Davalli, L. Scaglia, D. H. Zangen, J. Hollister, S. Bonner-Weir, and G. C. Weir, "Vulnerability of Islets in the Immediate Posttransplantation Period. Dynamic Changes in Structure and Function," *Diabetes* 45, no. 9 (1996): 1161–1167.

5. E. Zoneff, Y. Wang, C. Jackson, et al., "Controlled Oxygen Delivery to Power Tissue Regeneration," *Nature Communications* 15, no. 1 (2024): 4361.

6. R. Augustine, M. Gezek, N. S. Bostanci, A. Nguyen, and G. Camci-Unal, "Oxygen-Generating Scaffolds: One Step Closer to the Clinical Translation of Tissue Engineered Products," *Chemical Engineering Journal* 455, no. Pt 2 (2023): 140783.

7. D. Han and A. J. Steckl, "Coaxial Electrospinning Formation of Complex Polymer Fibers and Their Applications," *ChemPlusChem* 84, no. 10 (2019): 1453–1497.

8. A. Memic, T. Abdullah, H. S. Mohammed, K. Joshi Navare, T. Colombani, and S. A. Bencherif, "Latest Progress in Electrospun Nanofibers for Wound Healing Applications," *ACS Applied Bio Materials* 2, no. 3 (2019): 952–969.

9. M. M. Stevens and J. H. George, "Exploring and Engineering the Cell Surface Interface," *Science* 310, no. 5751 (2005): 1135–1138.

10. S. P. Hopkins, J. Pant, M. J. Goudie, D. T. Nguyen, and H. Handa, "Electrospun Bioabsorbable Fibers Containing S-Nitrosoglutathione for Tissue Engineering Applications," *ACS Applied Bio Materials* 3, no. 11 (2020): 7677–7686.

11. F. Zhou, M. Wen, P. Zhou, et al., "Electrospun Membranes of PELCL/PCL-REDV Loading With miRNA-126 for Enhancement of Vascular Endothelial Cell Adhesion and Proliferation," *Materials Science & Engineering, C: Materials for Biological Applications* 85 (2018): 37–46.

12. D. Han, M. Sasaki, H. Yoshino, S. Kofuji, A. T. Sasaki, and A. J. Steckl, "In-Vitro Evaluation of MPA-Loaded Electrospun Coaxial Fiber Membranes for Local Treatment of Glioblastoma Tumor Cells," *Journal of Drug Delivery Science and Technology* 40 (2017): 45–50.

13. Z. Man, L. Yin, Z. Shao, et al., "The Effects of Co-Delivery of BMSC-Affinity Peptide and rhTGF-Beta 1 From Coaxial Electrospun Scaffolds on Chondrogenic Differentiation," *Biomaterials* 35, no. 19 (2014): 5250–5260.

14. T. Abdullah, K. Gauthaman, A. H. Hammad, et al., "Oxygen-Releasing Antibacterial Nanofibrous Scaffolds for Tissue Engineering Applications," *Polymers* 12, no. 6 (2020): 1233.

15. M. Aleemardani, A. Solouk, S. Akbari, M. M. Dehghan, and M. Moeini, "Silk-Derived Oxygen-Generating Electrospun Patches for Enhancing Tissue Regeneration: Investigation of Calcium Peroxide Role and Its Effects on Controlled Oxygen Delivery," *Materialia* 14 (2020): 100877.

16. Z. Azine, M. Moeini, A. Solouk, and S. Akbari, "Polyurethane-Calcium Peroxide Composite Nanofibrous Scaffolds With Controlled Oxygen Release for Tissue Engineering Applications," *Nano: Brief Reports and Reviews* 18, no. 2 (2023): 2350012.

17. S. Khorshidi, A. Karkhaneh, and S. Bonakdar, "Oxygen-Releasing Nanofibers for Breathable Bone Tissue Engineering Application," *Journal of Biomaterials Applications* 35, no. 1 (2020): 72–82.

18. K. R. McCormac and M. J. Beazley, "Fabrication and Characterization of Biodegradable Oxygen-Releasing Micromaterials for Treatment of Hypoxic Environmental Waters," *Journal of Environmental Chemical Engineering* 8, no. 4 (2020): 103979.

19. J. Wang, Y. Zhu, H. K. Bawa, et al., "Oxygen-Generating Nanofiber Cell Scaffolds With Antimicrobial Properties," *ACS Applied Materials & Interfaces* 3, no. 1 (2011): 67–73.

20. A. Azari, A. Rahimi, M. Rajabibazl, H. A. Abbaszadeh, S. Hosseinzadeh, and A. Rahimpour, "Evaluation of In Vitro Coculture of Keratinocytes Derived From Foreskin and Adipose-Derived Mesenchymal Stem Cells (AMSCs) on a Multilayer Oxygen-Releasing Electrospun Scaffold Based on PU/PCL.Sodium Percarbonate (SPC)-Gelatine/PU," *Cell Biochemistry and Function* 41, no. 4 (2023): 434–449.

21. R. Samanipour, S. Farzaneh, J. Ranjbari, S. Hashemi, A. Khojasteh, and S. Hosseinzadeh, "Osteogenic Differentiation of Pulp Stem Cells From Human Permanent Teeth on an Oxygen-Releasing Electrospun Scaffold," *Polymer Bulletin* 80, no. 2 (2023): 1795–1816.

22. M. Zehra, W. Zubairi, A. Hasan, et al., "Oxygen Generating Polymeric Nano Fibers That Stimulate Angiogenesis and Show Efficient Wound Healing in a Diabetic Wound Model," *International Journal of Nanomedicine* 15 (2020): 3511–3522.

23. Y. Zheng, B. Xue, B. Wei, et al., "Core-Shell Oxygen-Releasing Fibers for Annulus Fibrosus Repair in the Intervertebral Disc of Rats," *Materials Today Bio* 18 (2023): 100535.

24. T. Ma, Y. Yang, X. Quan, et al., "Oxygen Carrier in Core-Shell Fibers Synthesized by Coaxial Electrospinning Enhances Schwann Cell Survival and Nerve Regeneration," *Theranostics* 10, no. 20 (2020): 8957–8973.

25. T. Agarwal, S. Kazemi, M. Costantini, et al., "Oxygen Releasing Materials: Towards Addressing the Hypoxia-Related Issues in Tissue Engineering," *Materials Science and Engineering: C* 122 (2021): 111896.

26. H. Wang, Y. Zhao, T. Li, Z. Chen, Y. Wang, and C. Qin, "Properties of Calcium Peroxide for Release of Hydrogen Peroxide and Oxygen: A Kinetics Study," *Chemical Engineering Journal* 303 (2016): 450–457.

27. M. H. Tootoonchi, M. Hashempour, P. L. Blackwelder, and C. A. Fraker, "Manganese Oxide Particles as Cytoprotective, Oxygen Generating Agents," *Acta Biomaterialia* 59 (2017): 327–337.

28. G. Camci-Unal, N. Alemdar, N. Annabi, and A. Khademhosseini, "Oxygen-Releasing Biomaterials for Tissue Engineering," *Polymer International* 62, no. 6 (2013): 843–848.

29. M. Gholipourmalekabadi, S. Zhao, B. S. Harrison, M. Mozafari, and A. M. Seifalian, "Oxygen-Generating Biomaterials: A New, Viable Paradigm for Tissue Engineering?," *Trends in Biotechnology* 34, no. 12 (2016): 1010–1021.

30. M. D. Menger, S. Jaeger, P. Walter, G. Feifel, F. Hammersen, and K. Messmer, "Angiogenesis and Hemodynamics of Microvasculature of Transplanted Islets of Langerhans," *Diabetes* 38, no. Suppl 1 (1989): 199–201.

31. P. Vajkoczy, A. M. Olofsson, H. A. Lehr, et al., "Histogenesis and Ultrastructure of Pancreatic Islet Graft Microvasculature. Evidence for Graft Revascularization by Endothelial Cells of Host Origin," *American Journal of Pathology* 146, no. 6 (1995): 1397–1405.

32. YSI, "Dissolved Oxygen Tables," Technical Instructions XA00055.

33. K.-M. Shang, H. Kato, N. Gonzalez, F. Kandeel, Y.-C. Tai, and H. Komatsu, "A Novel Approach to Determine the Critical Survival Threshold of Cellular Oxygen Within Spheroids via Integrating Live/Dead Cell Imaging With Oxygen Modeling," *American Journal of Physiology-Cell Physiology* 326, no. 4 (2024): C1262–C1271.

34. C. S. Schlosser, S. Brocchini, and G. R. Williams, "Stable Dried Catalase Particles Prepared by Electrospraying," *Nanomaterials* 12, no. 14 (2022): 2484.

35. N. Ferrara and W. J. Henzel, "Pituitary Follicular Cells Secrete a Novel Heparin-Binding Growth Factor Specific for Vascular Endothelial Cells," *Biochemical and Biophysical Research Communications* 161, no. 2 (1989): 851–858.

36. A. M. Shapiro, C. Ricordi, B. J. Hering, et al., "International Trial of the Edmonton Protocol for Islet Transplantation," *New England Journal of Medicine* 355 (2006): 13.

37. A. M. J. Shapiro, J. R. T. Lakey, E. A. Ryan, et al., "Islet Transplantation in Seven Patients With Type 1 Diabetes Mellitus Using a Glucocorticoid-Free Immunosuppressive Regimen," *New England Journal of Medicine* 343, no. 4 (2000): 230–238.

38. A. Rezania, J. E. Bruin, P. Arora, et al., "Reversal of Diabetes With Insulin-Producing Cells Derived In Vitro From Human Pluripotent Stem Cells," *Nature Biotechnology* 32, no. 11 (2014): 1121–1133.

39. G. G. Nair, J. S. Liu, H. A. Russ, et al., "Recapitulating Endocrine Cell Clustering in Culture Promotes Maturation of Human Stem-Cell-Derived β Cells," *Nature Cell Biology* 21, no. 2 (2019): 263–274.

40. N. Lifson, C. V. Lassa, and P. K. Dixit, "Relation Between Blood Flow and Morphology in Islet Organ of Rat Pancreas," *American Journal of Physiology. Endocrinology and Metabolism* 249, no. 1 (1985): E43–E48.

41. V. L. W. Go, ed., *The Pancreas: Biology, Pathobiology, and Disease*, 2nd ed. (Raven Press, 1993).

42. R. L. F. Amaral, M. Miranda, P. D. Marcato, and K. Swiech, "Comparative Analysis of 3D Bladder Tumor Spheroids Obtained by Forced Floating and Hanging Drop Methods for Drug Screening," *Frontiers in Physiology* 8 (2017).

Supporting Information

Additional supporting information can be found online in the Supporting Information section. **Figure S1:** Coaxial fiber electrospinning for formation of core-sheath fibers. **Figure S2:** pH measurements were performed using a SevenMulti pH meter (Mettler-Toledo AG, Switzerland). **Figure S3:** Culture setup of INS-1 spheroids seeded on the nanofiber membrane.

SUPPLEMENTARY INFORMATION

Fig. S1 – Coaxial fiber electrospinning for formation of core-sheath fibers. Core: PCL/PVP polymer incorporating CPO and lysozyme; Sheath: PEO polymer incorporating catalase. Created with Biorender.

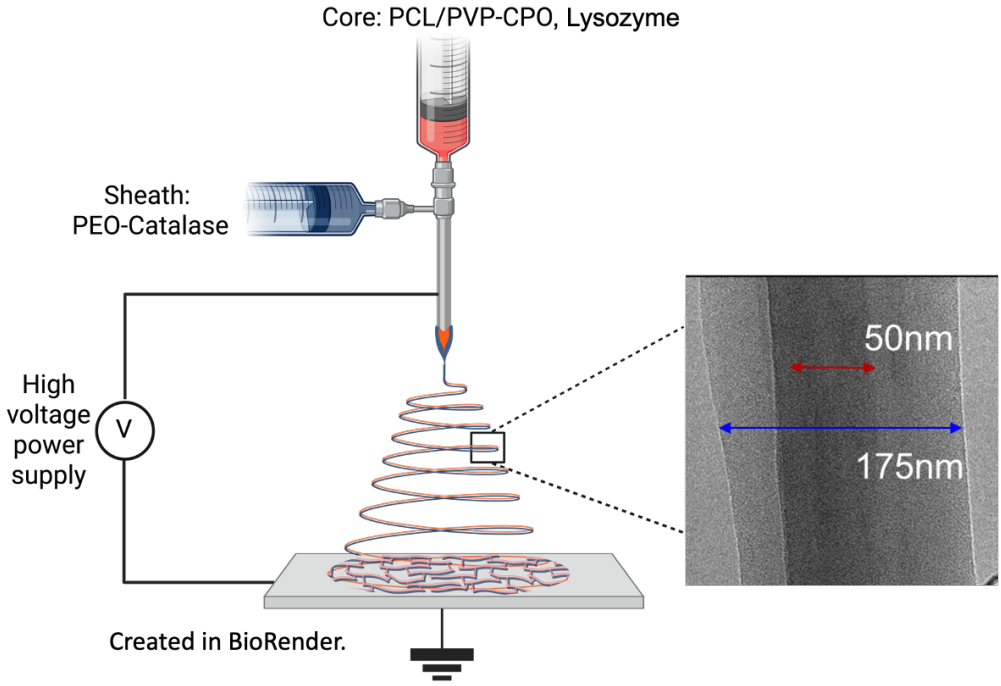

Fig. *S2 - pH measurements were performed using a SevenMulti pH meter (Mettler-Toledo AG, Switzerland). Because the pH probe required a minimum solution volume of 14 mL for accurate measurements, the membrane size was proportionally increased to 18.5 × 18.5 mm to maintain the same membrane-to-solution ratio used in the main study (49 mm² membrane per 2 mL of solution). Each membrane was immersed in 14 mL of either DPBS and deionized water. Three experimental groups (Control, CPO, and CPO + Catalase) were evaluated in triplicate (n = 3), and pH was monitored for 9 days at room temperature.*

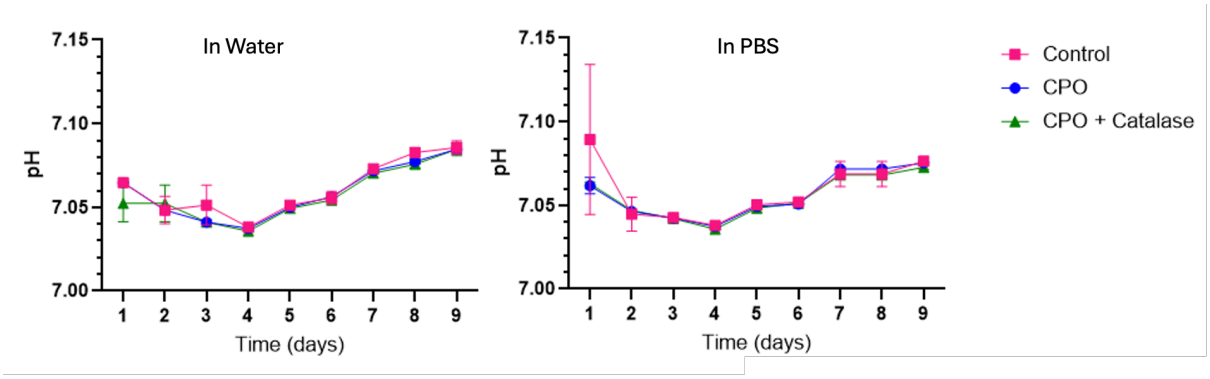

Fig. S3 - Culture setup of INS-1 spheroids seeded on the nanofiber membrane.
(a) Overview of the culture configuration. A 6 × 6 mm nanofiber membrane was placed at the bottom of a 96-well plate, and pre-formed INS-1 spheroids were seeded directly onto the membrane (left). A schematic cross-section illustrates the position of the spheroids on the upper surface of the nanofiber membrane during culture (right).
(b) Representative top-view micrographs of spheroids on the nanofiber membrane acquired using an Olympus IX51 microscope (Olympus, Tokyo, Japan). Fluorescence images of FDA-stained spheroids and bright-field images of the nanofiber membrane were acquired from the same field and merged to visualize the spatial relationship between the spheroids and membrane (left). An enlarged view demonstrates the close association between the spheroid and underlying nanofibers (right). Scale bars = 100 µm.